Journal of Computational Acoustics, Vol. 5, No. 4 (1997) 383–402

FINITE ELEMENT SOLUTION FOR WAVE PROPAGATION IN LAYERED FLUIDS

TONY W. H. SHEU* and C. C. FANG†
Department of Naval Architecture and Ocean Engineering,
National Taiwan University, 73 Chou-Shan Rd., Taipei, Taiwan, Republic of China

Received 6 December 1996
Revised 7 April 1997

A hyperbolic equation is considered for the propagation of pressure disturbance waves in layered fluids having different fluid properties. For acoustic problems of this sort, the characteristic finite element model alone does not suffice to ensure prediction of the monotonic wave profile across fluids having different properties. A flux corrected transport solution algorithm is intended for incorporation into the underlying Taylor–Galerkin finite element framework. The advantage of this finite element approach, in addition to permitting oscillation-free solutions, is that it avoids the necessity of dealing with medium discontinuity. As an analysis tool, the proposed monotonic finite element model has been intensively verified through problems which are amenable to analytic solutions. In modeling wave propagation in layered fluids, we have investigated the influence of the degree of medium change on the finite element solutions. Also, different finite element solutions are considered to show the superiority of using the flux corrected transport Taylor–Galerkin finite element model.

1. Introduction

Acoustics deals with the propagation of waves of finite amplitudes in fluid media. This long-established area has been among the subjects of interest to scientists for years, and has a strong association with the subject of unsteady gas dynamics. Considerable effort has been directed towards studying the propagation of disturbances in surroundings due to its practical relevance to the daily life of human beings. In the acoustic community, many of the previous endeavors have focused on small-amplitude wave propagation in homogeneous media. Since living standards are continuously improving, people have begun to call for a reduction in environmental noise. To meet the regulation of classification societies and the concerned regulatory bodies, researchers are encouraged to consider wave propagation in layered fluids.

As a first step towards extending our understanding of wave propagation in an environment involving different kinds of media, in this paper we deal with the propagation of small

*Professor
†Ph.D candidate

disturbances. The theory of linear hyperbolic partial differential equations of the second order constitutes the theoretical foundation of exploring this area of physics. Since wave propagation of finite amplitude is akin to the nonlinear theory of the steady flow of a compressible fluid, which involves first order hyperbolic equations, it is hoped that achievements made thus far can be transplanted into this area. As such, technological development in gas dynamics could be useful in bridging the gap between these two closely-related areas. In addition, from the computational standpoint, equations involving lower derivative orders are favored since they permit the use of lower-order interpolation polynomials to span the finite element space. Another important point to note is that it is advantageous to deal with lower-order derivatives because differentiation of equations is a primary source of discretization errors.

With the advent of high-speed computers and ever-improving cost effective performance, the use of analysis tools underlying computational acoustics has become widespread. It has also led to insights into propagation complexities. Although there is considerable literature concerning small-amplitude traveling waves in a homogeneous environment, little work has been done on the corresponding inhomogeneous case. The present work was undertaken largely in response to the need for further information on the wave characteristics when a wave impinges an interface across which fluid properties vary. Since finite elements have ostensible advantages, including geometric flexibility, application versatility, and automatic implementation of boundary conditions of the Neumann type, we adopt, among the applicable discretization alternatives, the finite element method. Besides these advantages, finite element analysis also has a mathematical foundation to prove the convergence of solutions. The use of the finite element method in modeling wave propagation is on the rise in the field of acoustics.

In the present work, we are led to formulate a well-posed differential system to model pressure waves propagating in layered fluids with abruptly varying fluid properties. We will derive in detail the target equation in Sec. 2. The goal of studying this problem is to gain an understanding of acoustic waves. We will present in Sec. 3 a newly developed high-order Taylor–Galerkin finite element model, followed by a comprehensive study of this model. In Sec. 4, we will address fundamental studies, including modified equation analysis, the amplification factor of the scheme, and the constraint conditions that permit monotonic solutions to be present in the hyperbolic system. In attempting to capture a sharp wave form in regions near the medium discontinuity, we adopt a higher-order Taylor–Galerkin finite element model. The erroneous numerical fluxes which yield oscillatory solutions are filtered out using the flux corrected transport (FCT) technique. This technique will be described in detail in Sec. 5. In Sec. 6 we will present several example problems to validate the proposed TG-FCT finite element model. Finally, we will draw a conclusion in Sec. 7 based on the problems considered and the results obtained.

2. Mathematical Model

As a first step towards studying propagation characteristics for the case where the fluid properties and, hence, wave speeds are discontinuous across an interface, we will focus our

attention only on waves with small amplitudes. In circumstances where the propagation character can be well-modeled by a linearized Euler equation, the incremental change of pressure disturbance $p(x, t)$ in layered fluids is governed by the following one-dimensional hyperbolic equation:

$$\frac{\partial}{\partial t}\left(\frac{1}{\rho c^2}\frac{\partial p}{\partial t}\right) - \frac{\partial}{\partial x}\left(\frac{1}{\rho}\frac{\partial p}{\partial x}\right) = 0\,. \tag{1}$$

In the above hyperbolic system, $\rho(x)$ is the medium density. Without loss of generality, we assume that the acoustic speed $c(x)$ is piecewise constant in the solution domain.

In attempting to derive a differential system which is equivalent to Eq. (1), we introduce two auxiliary variables to reduce the differentiation order:

$$m(x, t) = \frac{\partial p}{\partial t} + c\frac{\partial p}{\partial x}\,, \tag{2}$$

$$n(x, t) = \frac{\partial p}{\partial t} - c\frac{\partial p}{\partial x}\,. \tag{3}$$

By taking a partial differentiation of $m(x, t)$ with respect to both t and x, we can rederive the differential Eq. (1) on the condition that the following equation holds:

$$\frac{\partial m}{\partial t} - c(x)\frac{\partial m}{\partial x} = 0\,. \tag{4}$$

To achieve the same goal, we can take another auxiliary variable $n(x, t)$ into consideration. Parallel to the above differentiation procedures, we can show that the following first-order equation is also equivalent to Eq. (1):

$$\frac{\partial n}{\partial t} + c(x)\frac{\partial n}{\partial x} = 0\,. \tag{5}$$

For the case with a positive value of c, Eqs. (2) and (4) are sufficient to simulate waves traveling along either the positive or negative direction. For a right-traveling wave, Eq. (2) turns out to be $\frac{\partial p}{\partial t} + c\frac{\partial p}{\partial x} = 0$, which is sufficient to simulate the wave propagation. For simulation of left-traveling waves, Eqs. (2) and (4) are needed to model the wave characteristics. As in the case with a positive propagation speed, Eqs. (3) and (5) are sufficient to simulate left- or right-running waves. For the case with a negative propagating speed, the reduced form of Eq. (3), namely $\frac{\partial p}{\partial t} - c\frac{\partial p}{\partial x} = 0$, is sufficient to simulate a wave propagating along the negative direction. Notice that the source term $m(x, t)$ in Eq. (2) may be too large to avoid numerical difficulties. As a result, we would not use Eqs. (2) and (4) to model a wave propagating along the negative direction. Likewise, we would not consider Eqs. (3) and (5) to simulate a wave traveling along the positive direction. Now, it is appropriate to conclude that we can use the following equations to simulate a wave traveling along different directions:

$$\frac{\partial p}{\partial t} + c\frac{\partial p}{\partial x} = 0 \quad \text{for the positive-traveling wave}\,, \tag{6}$$

$$\frac{\partial p}{\partial t} - c\frac{\partial p}{\partial x} = 0 \quad \text{for the negative-traveling wave}\,. \tag{7}$$

It is also important to note that the necessary-and-sufficient condition which ensures equivalence between Eq. (1) and Eqs. (6) and (7) is that the acoustic speed c and the medium density ρ are piecewise constant. This implies that Eqs. (6) and (7) suffice to replace Eq. (1) in each domain of x where c is a constant. It remains for us to deal with the medium discontinuous point. We will discuss this issue in Sec. 6.2.

We will now extend the scope of analysis to the simulation of wave propagation across an interface. The simplest setting in this regard is depicted in Fig. 1. On the left side of the interface, defined in $x_a \leq x < x_0$, we designate the medium as "1", while the medium on the right side of the interface, defined in $x_0 < x \leq x_b$, is labeled as "2". By definition, the spatial location at x_0 is termed the medium discontinuous point. The pressure disturbance waves $p_i(x, t)$ $(i = 1, 2)$ follow different differential equations in their respective spatial domains. For medium "1", the right-traveling incident wave is governed by the following equation:

$$\frac{\partial p_1}{\partial t} + c_1 \frac{\partial p_1}{\partial x} = 0 . \tag{8}$$

As for the left-running reflected wave, it is governed by

$$\frac{\partial p_{1R}}{\partial t} - c_1 \frac{\partial p_{1R}}{\partial x} = 0 \tag{9}$$

for $x \in [x_a, x_0)$. For medium "2", the right-traveling transmitted wave is governed by the following equation:

$$\frac{\partial p_2}{\partial t} + c_2 \frac{\partial p_2}{\partial x} = 0 \tag{10}$$

for $x \in (x_0, x_b]$. To close the above hyperbolic differential system, initial conditions at $t = 0$ are specified over the entire domain. As for the specification of jump conditions at the medium interface, x_0, additional details are given in Sec. 6.2.

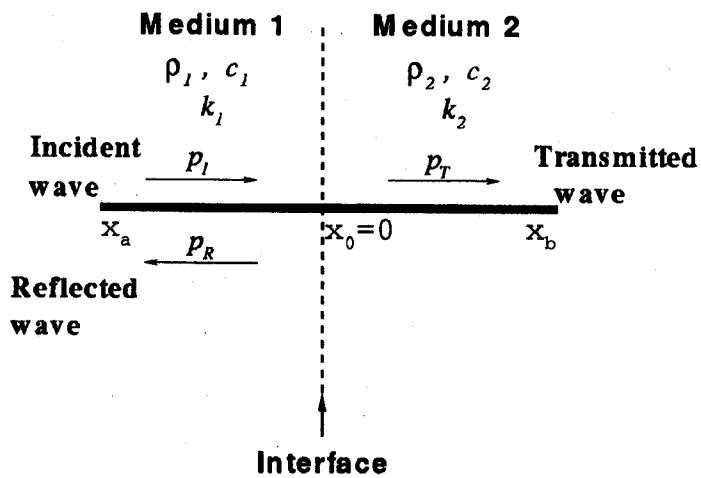

Fig. 1. An illustration of problem given in Sec. 6.2.

3. Numerical Model — Taylor–Galerkin Finite Element Model

In this study, we will focus on the conservation law form of the first-order hyperbolic equation. The equation considered is subjected to initial and boundary conditions

$$\frac{\partial \phi}{\partial t} + \frac{\partial f}{\partial x} = 0 . \tag{11}$$

Notice that the convective flux f shown above is given by

$$f(x, t) = c(x)\phi(x, t) . \tag{12}$$

The key to solving the above hyperbolic system is to introduce the characteristic features into the discrete system while conducting flux discretizations. There are many characteristic discretization schemes to choose from. Among these, the characteristic finite element method,[1] the discontinuous Galerkin method,[2] the discontinuity capturing SUPG method,[3] and the FCT finite element method[4,5] are most often referred to. It is not certain whether one approach which outperforms the others exists, and this is a subject of continuous investigation.

Following the essence of the Taylor–Galerkin model,[6] we expand the flux terms via Taylor series expansion, and then replace the higher-order time derivatives with the spatial derivatives. The inclusion of these higher-order terms brings in the hyperbolic property and, thus enhances scheme stability and also improves phase accuracy. Two main ingredients of the FCT solution algorithm will be constructed in this study.

In an attempt to retain variable orders of accuracy, we introduce four parameters, namely, α, β, γ and μ, into the Taylor series expansion:

$$\begin{aligned} f &= f^n + (t - t_n)\frac{\partial f}{\partial t}\bigg|^n + \frac{1}{2}(t - t_n)^2 \frac{\partial^2 f}{\partial t^2}\bigg|^n + \mathcal{O}((t - t_n)^3) \\ &= f^n + (t - t_n)\left(\alpha c \frac{\partial \phi}{\partial t} - \beta c \frac{\partial f}{\partial x}\right)\bigg|^n \\ &\quad -\frac{1}{2}(t - t_n)^2 \left(\gamma c^2 \frac{\partial^2 \phi}{\partial t \partial x} - \mu c^2 \frac{\partial^2 f}{\partial x^2}\right)\bigg|^n + \mathcal{O}((t - t_n)^3) . \end{aligned} \tag{13}$$

These parameters are not independently chosen, but are constrained by $\alpha + \beta = 1$ and $\gamma + \mu = 1$.

Having approximated the time-derivative terms, we proceed to discretize the remaining differential equations which involve only spatial derivatives by applying the Galerkin-weighted residuals model. For conducting the fundamental study of this semi-implicit approach, the problem considered is that with uniform grids of size h. By using the linear basis functions given by

$$N_j = \begin{cases} 1 + \dfrac{x - x_j}{h}; & \text{if } x \in [x_{j-1}, x_j] \\ 1 - \dfrac{x - x_j}{h}; & \text{if } x \in [x_j, x_{j+1}] \\ 0; & \text{otherwise} , \end{cases} \tag{14}$$

one can rewrite the discrete Taylor–Galerkin equation for $\delta\phi_J^n \equiv \phi_J^{n+1} - \phi_J^n$ as follows:

$$\left\{1 + \left[\frac{1}{2}\alpha\nu_{J+1/2} - \left(-\frac{1}{6} - \frac{1}{4}\alpha\nu_{J+1/2} + \frac{1}{6}\gamma\nu_{J+1/2}^2\right)\Delta^+\right]\right.$$
$$\left. + \left[-\frac{1}{2}\alpha\nu_{J-1/2} + \left(-\frac{1}{6} + \frac{1}{4}\alpha\nu_{J-1/2} + \frac{1}{6}\gamma\nu_{J-1/2}^2\right)\Delta^-\right]\right\}\delta\phi_J^n$$
$$= \frac{\Delta t}{\Delta x}\left[\left(-\frac{1}{2} + \frac{1}{2}\beta\nu_{J+1/2}\right)\Delta^+ - \left(\frac{1}{2} + \frac{1}{2}\beta\nu_{J-1/2}\right)\Delta^-\right] f_J^n\,, \tag{15}$$

where $\Delta x = h$, $\nu_{J+1/2} = c_{J+1/2}\Delta t/h$, $c_{J+1/2} = c(\phi_{J+1/2})$, $\phi_{J+1/2} = \frac{1}{2}(\phi_J + \phi_{J+1})$, $\Delta^+\phi_J^n \equiv \phi_{J+1}^n - \phi_J^n$, $\Delta^-\phi_J^n \equiv \phi_J^n - \phi_{J-1}^n$.

4. Fundamental Studies On The Taylor–Galerkin Finite Element Model

As Eq. (13) shows, the quality of the proposed Taylor–Galerkin formulation highly depends on four free parameters. The judicious determination of these values prompts us to conduct modified equation analysis. Referring to the Appendix, the corresponding modified equation for Eq. (15) is derived as follows:

$$\phi_t + c\phi_x = \frac{1}{2}c\nu\Delta x(\alpha + \beta - 1)\phi_{xx} + \frac{1}{12}c\nu^2(\Delta x)^2(2 - 3\alpha - 2\gamma)\phi_{xxx}$$
$$+ \left[\frac{1}{24}c\nu^3(\Delta x)^3(2\alpha + 2\gamma - 1) - \frac{1}{72}c\nu(\Delta x)^3(-3\beta - 6\alpha + 6)\right]\phi_{xxxx} + \cdots\,. \tag{16}$$

Here, $\nu \equiv c\Delta t/\Delta x$ is denoted as the Courant number.

Although it is cumbersome to derive the above modified equation, this fundamental study allows us to gain greater insight into the nature of the proposed discretization scheme, and enables us to achieve a solution with a higher accuracy order. Reduction of the numerical dissipation error dictates that the coefficients of the leading even derivative terms be equal to zero. This demands the values of α and β to be constrained as follows:

$$\alpha + \beta - 1 = 0\,. \tag{17}$$

In a similar manner, we can reduce the dispersion error by setting the coefficient of the third order derivative term to zero. This yields another identity for the values of the free parameters, α and γ:

$$2 - 3\alpha - 2\gamma = 0\,. \tag{18}$$

With the aid of this modified equation analysis, we can rationally assign the values of α, β, γ by virtue of Eqs. (17) and (18), from which a scheme having higher-order accuracy can be rendered. In this study, we choose $\alpha = \mu = 0$, $\beta = \gamma = 1$.

The amplification factor G and the phase angle Φ are respectively given by

$$G = 1 + \frac{\beta\nu^2(\cos\beta_x - 1) - i\nu\sin\beta_x}{\left[1 + \frac{1}{3}(1 - \gamma\nu^2)(\cos\beta_x - 1)\right] + i\frac{1}{2}\alpha\nu\sin\beta_x}\,, \tag{19}$$

$$\Phi = \tan^{-1} \frac{\mathrm{Im}(G)}{\mathrm{Re}(G)} . \tag{20}$$

In Eq. (19), $\beta_x = k_m \Delta x$, where $k_m = \frac{m\pi}{L}$, $m = 0, 1, 2, \ldots, M$. Here, M is the number of uniform intervals contained in a domain of length L. The modulus of the amplification factor is plotted in Fig. 2 for both high-order and low-order schemes. For completeness, we also plot the relative phase error for each scheme over a time step. As Fig. 3 reveals, leading and lagging phase errors may coexist.

Next, we wish to examine whether monotonic solutions can be computed from the proposed generalized Taylor–Galerkin finite element model. With this goal in mind, we rewrite Eq. (15) as follows:

$$\phi_J^{n+1} - \tilde{\mathbf{C}}_{J+1/2}\Delta^+\phi_J^{n+1} + \tilde{\mathbf{C}}_{J-1/2}\Delta^-\phi_J^{n+1} = \phi_J^n + \mathbf{C}_{J+1/2}\Delta^+\phi_J^n - \mathbf{C}_{J-1/2}\Delta^-\phi_J^n , \tag{21}$$

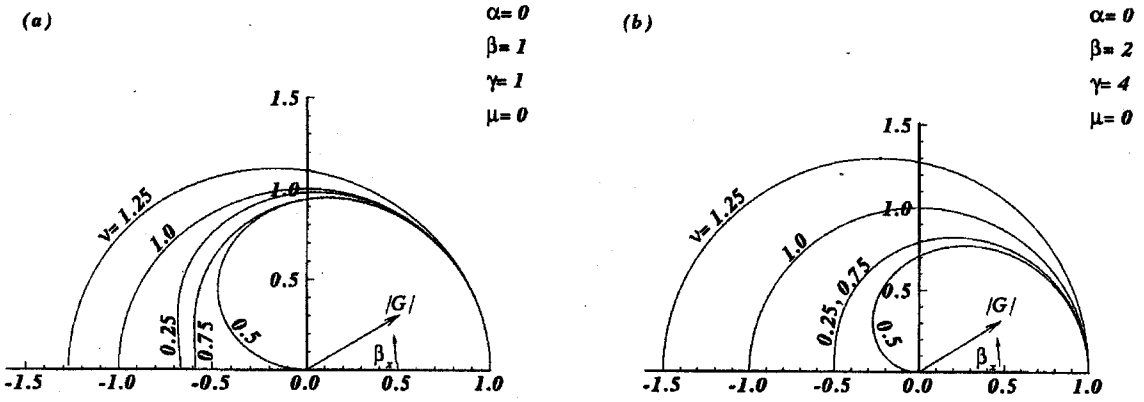

Fig. 2. The amplification factors of G for (a) the high order scheme; and (b) the low order scheme.

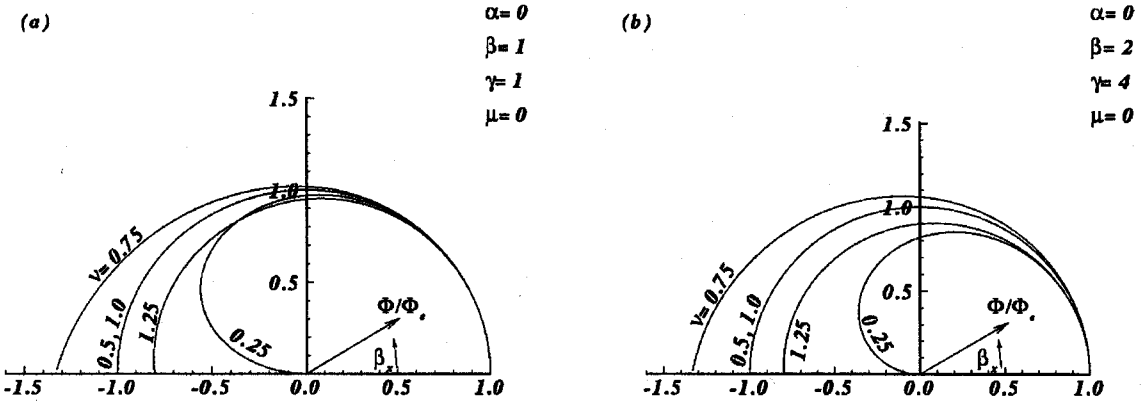

Fig. 3. The relative phase errors of Φ/Φ_e for (a) the high order scheme; and (b) the low order scheme.

where

$$\begin{aligned}
\tilde{\mathbf{C}}_{J+1/2} &= -\frac{1}{6} - \frac{1}{4}\alpha\nu + \frac{1}{6}\gamma\nu^2\,, \\
\tilde{\mathbf{C}}_{J-1/2} &= -\frac{1}{6} + \frac{1}{4}\alpha\nu + \frac{1}{6}\gamma\nu^2\,, \\
\mathbf{C}_{J+1/2} &= \frac{1}{6} + \frac{1}{4}(\alpha-2)\nu + \frac{1}{6}(3\beta-\gamma)\nu^2\,, \\
\mathbf{C}_{J-1/2} &= \frac{1}{6} - \frac{1}{4}(\alpha-2)\nu + \frac{1}{6}(3\beta-\gamma)\nu^2\,.
\end{aligned} \tag{22}$$

Subject to an initial condition of a monotonic type, the finite element solution can remain monotonic if $\sum_j |\phi_{j+1}^{n+1} - \phi_j^{n+1}| \le \sum_j |\phi_{j+1}^n - \phi_j^n|$. In what follows, we will apply the concept of TVD[7] (Total Variation Diminishing) to achieve solution monotonicity. Harten[8] showed that satisfaction of the following sufficient conditions, though not regarded as a necessary condition, ensures that monotonic solutions will be retained:

$$\tilde{\mathbf{C}}_{J+1/2} \ge 0\,, \quad \tilde{\mathbf{C}}_{J-1/2} \ge 0\,, \tag{23}$$

$$\mathbf{C}_{J+1/2} \ge 0\,, \quad \mathbf{C}_{J-1/2} \ge 0\,, \quad \mathbf{C}_{J+1/2} + \mathbf{C}_{J-1/2} \le 1\,. \tag{24}$$

According to the definitions of $\tilde{C}_{J\pm1/2}$ and $C_{j\pm1/2}$ given in Eq. (22), it is clear to us that employment of the high-order Taylor–Galerkin formulation where (α, β, γ, μ) = (0, 1, 1, 0) applies fails to reach the desirable constraint conditions given in Eqs. (23) and (24). This variable setting is, thus, inapplicable to a problem involving discontinuities. In this light, we were prompted to refine the present characteristic finite element model to capture discontinuities in the flow.

After conducting a lengthly mathematical exercise, we can show that the use of $\alpha = 0$, $\beta = \frac{1}{|\nu|}$, $\gamma = \frac{1}{\nu^2}$, and $\mu = 0$ can satisfy the TVD conditions given in Eqs. (23) and (24). The use of these chosen parameters results in the following modified equation:

$$\frac{\partial\phi}{\partial t} + \frac{\partial f}{\partial x} = \left(\frac{1}{|\nu|} - 1\right)(t - t_n)c\frac{\partial^2 f}{\partial x^2} + \frac{1}{2}\left(\frac{1}{\nu^2} - 1\right)(t - t_n)^2 c^2 \frac{\partial^3\phi}{\partial t \partial x^2}\,. \tag{25}$$

This implies that we can simply add some physically-relevant artificial viscosities to successfully suppress oscillations to assure solution monotonicity. While this artificial viscosity model closely resembles the proposed Taylor–Galerkin finite element model, it is noteworthy that this model is no longer classified as the Taylor–Galerkin model unless $\nu = 1$. The main reason is that $\alpha + \beta \ne 1$ and $\gamma + \mu \ne 1$. In summary, the variable flux discretization scheme presented here is considered to be effective since this model can provide not only high-order but also monotonic solutions.

5. Flux Corrected Transport (FCT) Algorithm

While the stability of the discrete hyperbolic system has been enhanced, the added artificial viscosities cause the accuracy to deteriorate. Very often, numerical spreading is too

excessive to allow an accurate prediction of the transport phenomenon. Thus, there is strong motivation to build a more accurate scheme while retaining good stability in regions containing high gradient profiles.

The monotone positivity-preserving scheme was first investigated by Boris and Book[9] who proposed the Flux-Corrected-Transport (FCT) solution algorithm. This algorithm was later generalized by Zalesak[10] and extended to multidimensional analyses. The idea behind this nonlinear flux correction method is to combine a high-order scheme with a low-order scheme so that the former can be used in smooth regions and the monotonic low-order scheme is in near discontinuities. Later, Erlebacher[11] and Parrot *et al.*[12] applied the FCT technique to finite element analysis. Motivated by the success of Löhner *et al.*,[13] the flux corrected transport technique of Boris and Book[9] will be employed in conjunction with the Taylor–Galerkin finite element model, to solve the linear hyperbolic system. The main solution steps are as follows:

1. We begin by choosing a set of parameters $(\alpha^{\mathbf{h}}, \beta^{\mathbf{h}}, \gamma^{\mathbf{h}}, \mu^{\mathbf{h}})$ for computing high-order solutions $\mathbf{U}^{\mathbf{h}}(= [\phi_1^{\mathbf{h}}, \phi_2^{\mathbf{h}}, \ldots, \phi_{N_{\text{dof}}}^{\mathbf{h}}]^{\mathrm{T}})$ from the following lumping-mass iteration procedures. The following iterative process continues until the convergence criterion given by $\max \left| \frac{\delta\phi^{\mathbf{h}}_{(p+1)} - \delta\phi^{\mathbf{h}}_{(p)}}{\delta\phi^{\mathbf{h}}_{(p+1)}} \right| \leq 10^{-2}$ is reached:

$$\begin{aligned} \delta\mathbf{U}^{\mathbf{h}}_{(0)} &= 0\,, \\ \delta\mathbf{U}^{\mathbf{h}}_{(p+1)} &= \bar{\mathbf{M}}^{-1}_{\mathbf{h}}[\mathbf{R}^{\mathbf{h}} - (\mathbf{M}_{\mathbf{h}} - \bar{\mathbf{M}}_{\mathbf{h}})\delta\mathbf{U}^{\mathbf{h}}_{(p)}] = [\mathbf{F}^{el^{\mathbf{h}}}]\,, \end{aligned} \tag{26}$$

where

$$\begin{aligned} \mathbf{M}_{\mathbf{h}} &= \mathbf{M}(\alpha^{\mathbf{h}}, \beta^{\mathbf{h}}, \gamma^{\mathbf{h}}, \mu^{\mathbf{h}})\,, \\ \mathbf{R}^{\mathbf{h}} &= \mathbf{R}(\alpha^{\mathbf{h}}, \beta^{\mathbf{h}}, \gamma^{\mathbf{h}}, \mu^{\mathbf{h}})\,, \\ \mathbf{M} &= [M_{IJ}] = \mathcal{A}_{el=1}^{n_{el}}(\mathbf{m}^{el})\,, \\ \bar{\mathbf{M}} &= [\bar{M}_{IJ}] = \mathcal{A}_{el=1}^{n_{el}}(\bar{\mathbf{m}}^{el})\,, \\ \mathbf{R} &= \mathcal{A}_{el=1}^{n_{el}}(\mathbf{r}^{el})\,, \\ (\bar{\mathbf{m}}^{el}) &= \mathrm{diag}(\bar{m}_i^{el})\,, \\ (\bar{m}_i^{el}) &= \sum_j m_{ij}^{el}\,, \end{aligned}$$

$$\begin{aligned} \mathbf{m}^{el} = [m_{ij}^{el}] = \Bigg[\int_{\Omega^{el}} \Bigg(N_i N_j - \frac{1}{2}\alpha c \Delta t \frac{\partial N_i}{\partial x} N_j + \frac{1}{6}\gamma c^2 \Delta t^2 \frac{\partial N_i}{\partial x}\frac{\partial N_j}{\partial x} \Bigg)\, d\Omega^{el} \\ - \Bigg(-\frac{1}{2}\alpha c \Delta t N_i N_j + \frac{1}{6}\gamma c^2 \Delta t^2 N_i \frac{\partial N_j}{\partial x} \Bigg) \Bigg|_{\Gamma} \Bigg]\,, \end{aligned}$$

$$\begin{aligned} \mathbf{r}^{el} = [r_i^{el}] = \Bigg[\int_{\Omega^{el}} \Bigg(\Bigg(\Delta t \frac{\partial N_i}{\partial x} N_j - \frac{1}{2}\beta c \Delta t^2 \frac{\partial N_i}{\partial x}\frac{\partial N_j}{\partial x} + \frac{1}{6}\mu c^2 \Delta t^3 \frac{\partial N_i}{\partial x}\frac{\partial^2 N_j}{\partial x^2} \Bigg) f_J^n \Bigg)\, d\Omega^{el} \\ - \Bigg(\Bigg(\Delta t N_i N_j - \frac{1}{2}\beta c \Delta t^2 N_i \frac{\partial N_j}{\partial x} + \frac{1}{6}\mu c^2 \Delta t^3 N_i \frac{\partial^2 N_j}{\partial x^2} \Bigg) f_J^n \Bigg) \Bigg|_{\Gamma} \Bigg]\,, \end{aligned}$$

$$F_i^{el^{\mathbf{h}}} = \bar{M}_{IJ_{\mathbf{h}}}^{-1}[r_i^{el^{\mathbf{h}}} - (m_{ij}^{el^{\mathbf{h}}} - \bar{m}_i^{el^{\mathbf{h}}}\delta_{ij})\delta\phi_{J_{(p)}}^{\mathbf{h}}]\,.$$

N_i and N_j in the above equations are the so-called weighting and shape functions, respectively. Ω is the domain of the element, Γ is the boundary of the element, N_{dof} is the number of unknowns, i, j are indices of the node of an element, J is the index of the node in the global sense, the supscript "el" indicates the number of elements, and $\mathcal{A}$ is the assembling operator.

2. By using $(\alpha^{\mathbf{l}}, \beta^{\mathbf{l}}, \gamma^{\mathbf{l}}, \mu^{\mathbf{l}})$, one can compute the low-order solutions $\mathbf{U}^{\mathbf{l}}(= [\phi_1^{\mathbf{l}}, \phi_2^{\mathbf{l}}, \ldots, \phi_{N_{\text{dof}}}^{\mathbf{l}}]^{\mathrm{T}})$ from the following lumping-mass procedures:

$$\delta\mathbf{U}^{\mathbf{l}} = \bar{\mathbf{M}}_{\mathbf{l}}^{-1}\mathbf{R}^{\mathbf{l}} = [\mathbf{F}^{el^{\mathbf{l}}}]\,. \tag{27}$$

Here, the anti-diffusive flux array $\mathbf{F}^{el^{\mathbf{l}}}$ is given by $\mathbf{F}^{el^{\mathbf{l}}} = \bar{\mathbf{M}}_{\mathbf{l}}^{-1}\mathbf{r}^{el^{\mathbf{l}}}$, where $\bar{\mathbf{M}}_{\mathbf{l}} = \bar{\mathbf{M}}(\alpha^{\mathbf{l}}, \beta^{\mathbf{l}}, \gamma^{\mathbf{l}}, \mu^{\mathbf{l}})$ and $\mathbf{R}^{\mathbf{l}} = \mathbf{R}(\alpha^{\mathbf{l}}, \beta^{\mathbf{l}}, \gamma^{\mathbf{l}}, \mu^{\mathbf{l}})$.

3. We then compute the anti-diffusive flux array $\mathbf{F}^{el}$ in each element as follows:

$$\mathbf{F}^{el} = \mathbf{F}^{el^{\mathbf{h}}} - \mathbf{F}^{el^{\mathbf{l}}} = (F_i^{el})\,, \tag{28}$$

where $F_i^{el} = \bar{M}_{IJ_{\mathbf{h}}}^{-1}[r_i^{el^{\mathbf{h}}} - (m_{ij}^{el^{\mathbf{h}}} - \bar{m}_i^{el^{\mathbf{h}}}\delta_{ij})\delta\phi_J^{\mathbf{h}}] - \bar{M}_{IJ_{\mathbf{l}}}^{-1}r_i^{el^{\mathbf{l}}}$.

4. The success of applying the FCT algorithm depends largely on the introduced antidiffusion term, which is not allowed to generate new maxima or minima in the solution. To avoid accentuation of the already-existing extrema, fluxes given in Eq. (28) are corrected as follows:

$$F_i^{el^{\mathbf{c}}} = s_i^{el} \cdot \max\{0, \min[|F_i^{el}|, \bar{s}_i^{el}\Delta^+\phi_{I+1}^{\mathbf{l}}, \bar{s}_i^{el}\Delta^-\phi_I^{\mathbf{l}}]\}\,, \tag{29}$$

where

$$s_i^{el} = \operatorname{sgn}(F_i^{el})\,,$$
$$\bar{s}_i^{el} = \begin{cases} \operatorname{sgn}(-F_i^{el}); & i = 1 \\ \operatorname{sgn}(F_i^{el}); & i = 2\,. \end{cases}$$

5. The finite element solution at time $t = t_{n+1}$ is then computed from

$$\mathbf{U}^{n+1} = \mathbf{U}^{\mathbf{l}} + \mathcal{A}_{el=1}^{n_{el}}(\mathbf{F}^{el^{\mathbf{c}}})\,, \tag{30}$$

where $\mathbf{F}^{el^{\mathbf{c}}} = [F_i^{el^{\mathbf{c}}}]$, $\mathbf{U}^{n+1} = [\phi_1^{n+1}, \phi_2^{n+1}, \ldots, \phi_{N_{\text{dof}}}^{n+1}]^{\mathrm{T}}$.

6. Numerical Results

For validation purposes, we will first benchmark the analysis code by solving problems which are amenable to analytical data. Here, we will assess the simulation quality by casting the

computed errors in their norm forms:

$$\|e\|_{L_1(\Omega)} = \int_\Omega |e| dx\,, \tag{31}$$

$$\|e\|_{L_2(\Omega)} = \left(\int_\Omega |e|^2 dx\right)^{\frac{1}{2}}\,, \tag{32}$$

$$L_\infty = \max_i |e_i|\,, \quad i = 1, 2, \ldots, n\,, \tag{33}$$

$$E_{\text{shp}} = \sum_{i=1}^{n-1} |e_{i+1} - e_i|\,. \tag{34}$$

Here, n is the total number of nodes considered, and e_i denotes the difference between the computed solution $\tilde{u}$ and the exact solution u.

6.1. *Validation test*

Consider the following equation for a disturbance propagating in a domain D bounded by two ends at $x = 1$ and $x = -1$:

$$\frac{\partial \phi}{\partial t} + c\frac{\partial \phi}{\partial x} = 0\,. \tag{35}$$

Three initial profiles were chosen to validate use of the proposed Taylor–Galerkin finite element model and the chosen FCT filtering technique.

The analysis is carried out under the conditions of the unit propagation speed and $(\alpha^{\text{h}}, \beta^{\text{h}}, \gamma^{\text{h}}, \mu^{\text{h}}) = (0, 1, 1, 0)$, $(\alpha^{\text{l}}, \beta^{\text{l}}, \gamma^{\text{l}}, \mu^{\text{l}}) = (0, 2, 4, 0)$. We terminate the calculation at $t = 1$ along with $\Delta t = 0.005$ and $\Delta x = 0.01$. Given the initial profile

$$\phi_1(0, x) = \phi_1(x) = \begin{cases} 0; & x \in [-1, -0.8] \\ \cos\left[\dfrac{5}{3}\pi(x + 0.5)\right]; & x \in (-0.8, -0.2) \\ 0; & x \in [-0.2, 1] \end{cases}, \tag{36}$$

the cosine wave profile is plotted at $t = 1$. From Fig. 4, the merit and the drawback of the high- and low-order Taylor–Galerkin schemes are apparent to the present authors. The solution computed from the high-order scheme is nominally indistinguishable from the analytic solution, except in regions near the root of the solution profile. It is notable that the filtering procedure is dispensable in this test profile.

In order to demonstrate the effectiveness of the proposed advection scheme in resolving discontinuities, we will considered the following square profile:

$$\phi_2(0, x) = \phi_2(x) = \begin{cases} 0; & x \in [-1, -0.8] \\ 1; & x \in (-0.8, -0.2) \\ 0; & x \in [-0.2, 1] \end{cases}. \tag{37}$$

Figure 5(a) clearly shows that low-order solutions are grossly contaminated by numerical spreading. In the high-order solution, erroneous oscillations, as shown in Fig. 5(b), are

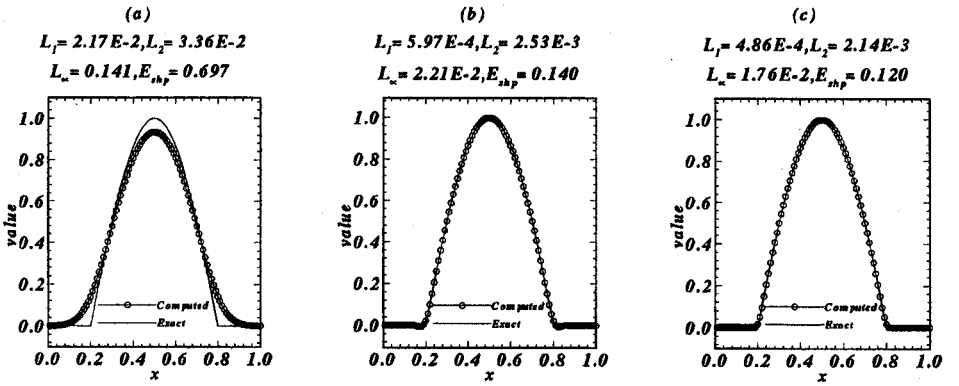

Fig. 4. The computed cosine wave profiles by (a) the low-order scheme; (b) the high-order scheme; and (c) the FCT scheme.

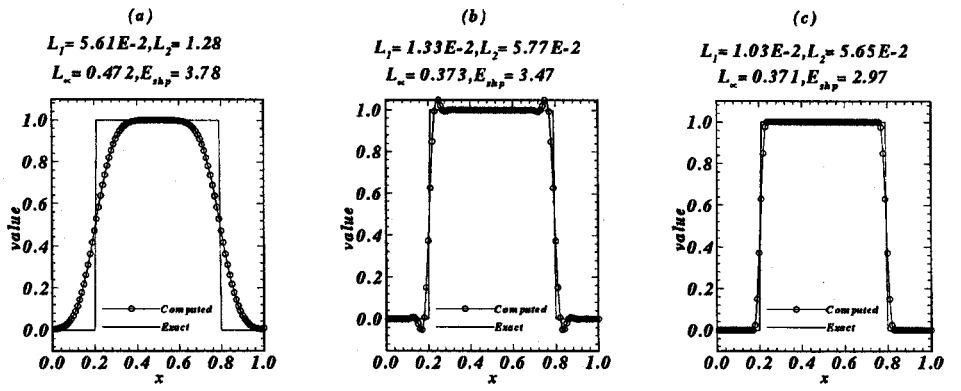

Fig. 5. The computed square wave profiles by (a) the low-order scheme; (b) the high-order scheme; and (c) the FCT scheme.

apparent near the jumps. On the other hand, as seen in Fig. 5(c), these wiggles have been well-suppressed by using the flux corrected transport technique.

We will now deal with a more challenging problem. The problem is that of the following semi-elliptic initial profile form:

$$\phi_3(0, x) = \phi_3(x) = \begin{cases} 0; & x \in [-1, -0.8] \\ \left(1 - \dfrac{100}{9}(x + 0.5)^2\right)^{\frac{1}{2}}; & x \in (-0.8, -0.2) \\ 0; & x \in [-0.2, 1] \end{cases} \cdot \tag{38}$$

Specific to this profile, there exists a jump at the root above which the solution follows a continuous curve. The use of a lower-order scheme, while making the computed solutions more stable, adds excessive viscosity to the formulation and, thus, makes the scheme overly diffusive. From the computed solutions shown in Fig. 6, we realize that the FCT solution is not only monotonic, but also accurate.

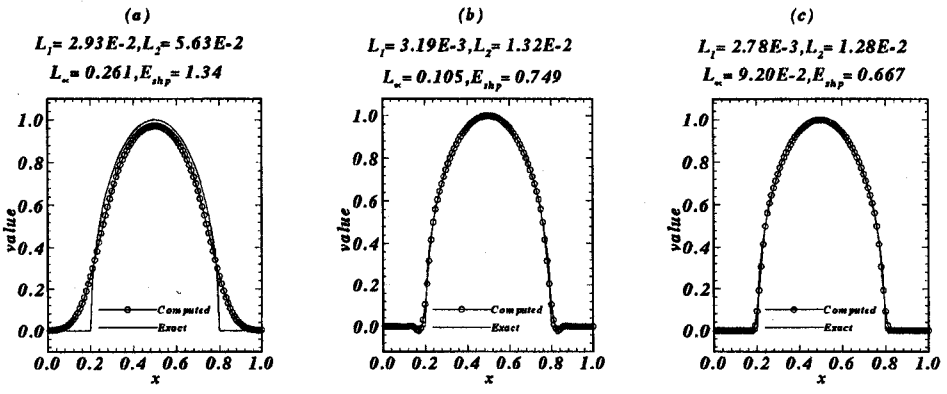

Fig. 6. The computed semi-elliptic wave profiles by (a) the low-order scheme; (b) the high-order scheme; and (c) the FCT scheme.

6.2. *Wave propagation across a medium interface*

The success in applying the TG-FCT scheme to the wave propagation problems given in Sec. 6.1 encourages us to conduct numerical simulations of wave propagation in layered fluids. For this study, we will confine our attention to a single wave which travels through layered fluids. Across an interface in layered fluids, fluid properties change abruptly.

When an incident wave in the fluid medium "1" with a density ρ_1 and speed of sound c_1 impinges on the boundary of a contiguous medium with a density ρ_2 and speed of sound c_2, a reflected wave is generated in medium "1", and a transmitted wave travels continuously through medium "2". Depending on the characteristic impedances of the media considered, as defined by $\rho_i c_i$ $(i = 1, 2)$, and the angle of incidence of the incident wave, the amplitudes and phases of the reflected and transmitted waves vary upon striking the interface of the two media. In the limiting case, the medium impedance remains as the sole determining factor in the single dimension analysis. As seen in Fig. 1, the incident wave having a frequency of ω travels along the positive direction in medium "1". The wave considered is represented by

$$p_I = p_i e^{I(\omega t - k_1 x)}\,, \tag{39}$$

where p_i is the pressure disturbance amplitude of the wave and $k_1 (\equiv \omega/c_1)$ is the wavelength. As is usual, we assume that the transmitted wave retains the same frequency as does the incident wave. Thus, the reflected and transmitted waves read respectively as:

$$p_R = p_r e^{I(\omega t + k_1 x)}\,, \tag{40}$$

$$p_T = p_t e^{I(\omega t - k_2 x)}\,. \tag{41}$$

On the medium interface, physical reasons demand that pressure disturbance computed from two sides approach the same value. Enforcement of this jump condition yields

$$p_i + p_r = p_t\,. \tag{42}$$

According to the definition of impedance, together with the associated particle velocities v_I, v_R and v_T which follow the relation $v_I + v_R = v_T$ at the medium interface, we have

$$\frac{p_I}{\rho_1 c_1} - \frac{p_R}{\rho_1 c_1} = \frac{p_T}{\rho_2 c_2}, \tag{43}$$

or

$$\rho_2 c_2 (p_I - p_R) = \rho_1 c_1 p_T . \tag{44}$$

By substituting expressions for p_I, p_R, and p_T, as defined in Eqs. (39)–(41), we can rewrite Eq. (44) at the medium interface as

$$\rho_2 c_2 (p_i - p_r) = \rho_1 c_1 p_t . \tag{45}$$

Eliminating p_t from Eqs. (42) and (45) yields

$$p_r = p_i \frac{c_2\rho_2 - c_1\rho_1}{c_2\rho_2 + c_1\rho_1} . \tag{46}$$

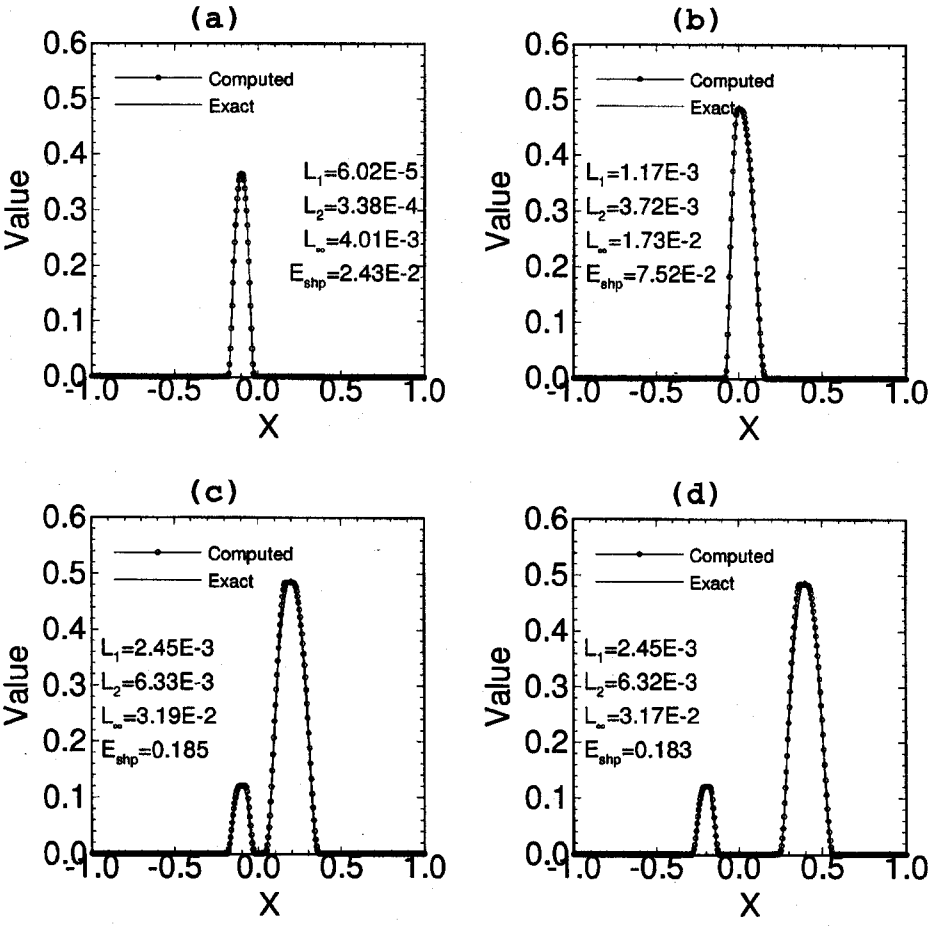

Fig. 7. The computed results for the case of $\rho_1 = \rho_2$ and $c_1 : c_2 = 1 : 2$. (a) $t = 0.1$; (b) $t = 0.2$; (c) $t = 0.3$; and (d) $t = 0.4$.

By using Eq. (42), we can determine p_t as

$$p_t = p_i + p_r = p_i \frac{2c_2\rho_2}{c_1\rho_1 + c_2\rho_2}. \tag{47}$$

Depending on the relative values of $c_1\rho_1$ and $c_2\rho_2$, the acoustic pressure of the reflected wave from the interface is either in phase or out of phase with that of the incident wave. According to Eq. (46), when the impedance of medium "2" is greater than that of medium "1", a positive excess pressure p in the incident wave is reflected as a positive excess pressure. Provided that $\rho_2 c_2 < \rho_1 c_1$, a positive excessive pressure in the incident wave is reflected as a negative excess pressure. With the aid of Eqs. (46) and (47), which are valid in the present linear system, and assuming an unchanged frequency for an incident wave passing through a medium interface, we can simulate the wave motion in layered fluids by means of superposition of individual waves in each medium.

As an illustration to show that the proposed characteristic flux discretization scheme is applicable to predicting pressure disturbance wave propagation across a medium interface,

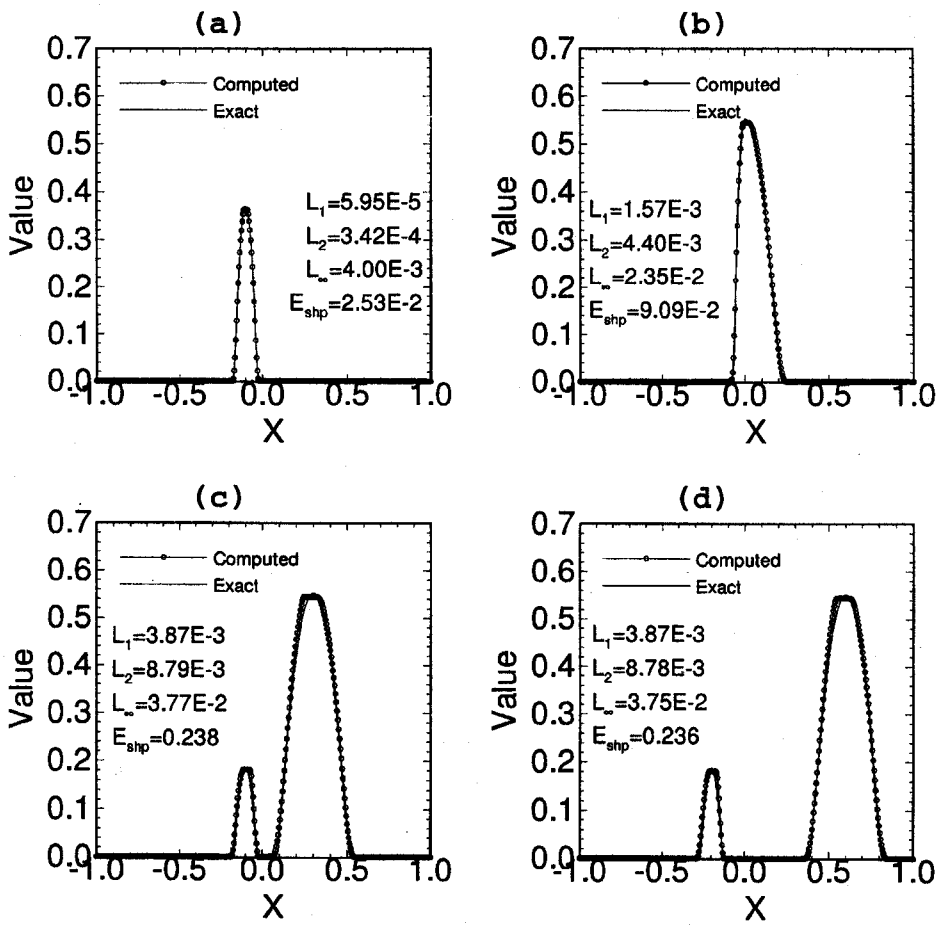

Fig. 8. The computed results for the case of $\rho_1 = \rho_2$ and $c_1 : c_2 = 1 : 3$. (a) $t = 0.1$; (b) $t = 0.2$; (c) $t = 0.3$; and (d) $t = 0.4$.

we will consider a condition which simplifies the analysis. In a domain of $-1 \leq x \leq 1$, the fluid properties are arranged as

$$\rho(x) = \begin{cases} \rho_1; & -1 \leq x \leq 0^-, \\ \rho_2; & 0^+ \leq x \leq 1, \end{cases} \tag{48}$$

and

$$c(x) = \begin{cases} c_1; & -1 \leq x \leq 0^-, \\ c_2; & 0^+ \leq x \leq 1. \end{cases} \tag{49}$$

The values of ρ_1, ρ_2 are equal to each other for all four cases considered in this study. For simplicity, we assign their values as 1. The values of c_1 and c_2 are arranged in ratios 1:2, 1:3, 1:1/2, and 1:1/3, respectively.

Initially, we assign the initial profile of p in Eq. (1) (equal to the superposition of p_i, p_r and p_t in Eqs. (8)–(10)) as g, which takes on the value of zero everywhere except in the

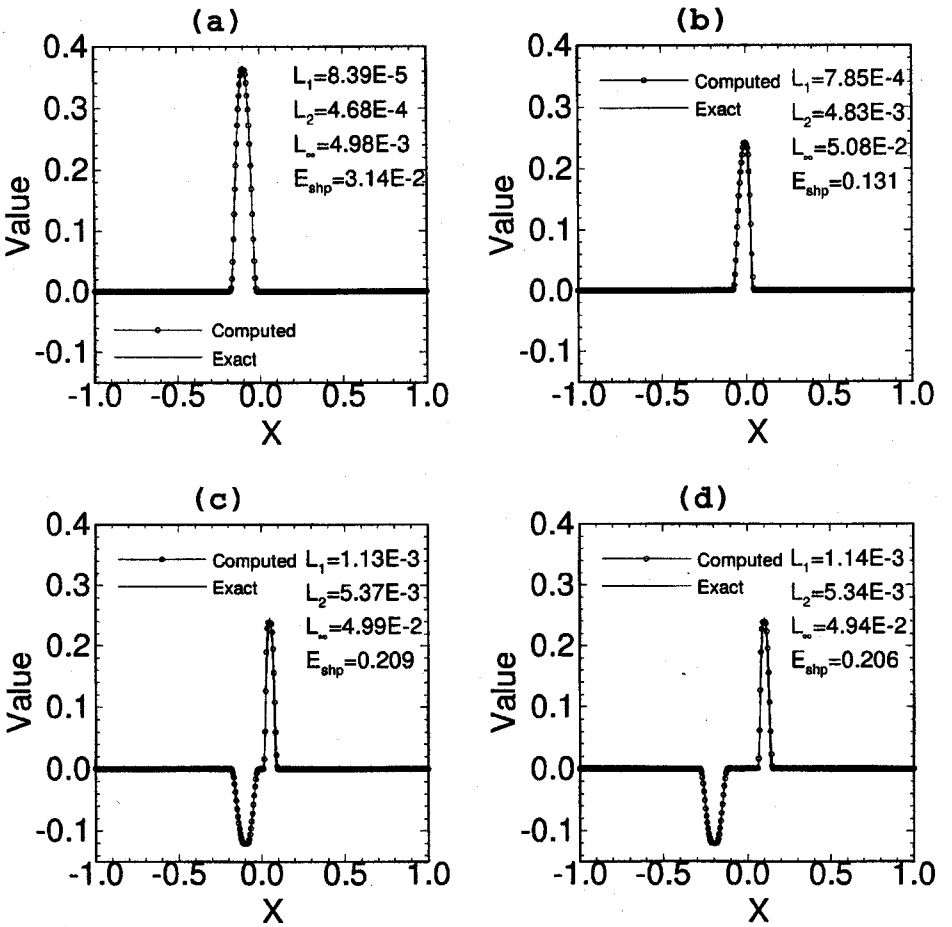

Fig. 9. The computed results for the case of $\rho_1 = \rho_2$ and $c_1 : c_2 = 1 : 1/2$. (a) $t = 0.1$; (b) $t = 0.2$; (c) $t = 0.3$; and (d) $t = 0.4$.

range of $(-0.3, -0.1)$, where

$$g(x) = \exp\left[\frac{1}{10^4(x+0.3)^2(x+0.1)^2}\right]. \tag{50}$$

This hyperbolic equation is amenable to analytic solution given by

$$p(x,t) = \begin{cases} g\left(\dfrac{x}{c_1} - t\right) + \dfrac{\rho_2 c_2 - \rho_1 c_1}{\rho_2 c_2 + \rho_1 c_1} g\left(-\dfrac{x}{c_1} - t\right), & -1 \le x \le 0^- \\ \dfrac{2\rho_2 c_2}{\rho_2 c_2 + \rho_1 c_1} g\left(\dfrac{x}{c_2} - t\right), & 0^+ \le x \le 1. \end{cases} \tag{51}$$

Figure 7 plots the finite element solutions which are computed under the conditions $\rho_1 : \rho_2 = 1 : 1$ and $c_1 : c_2 = 1 : 2$. The grid resolution is $\Delta x = 1/200$. Analytic solutions

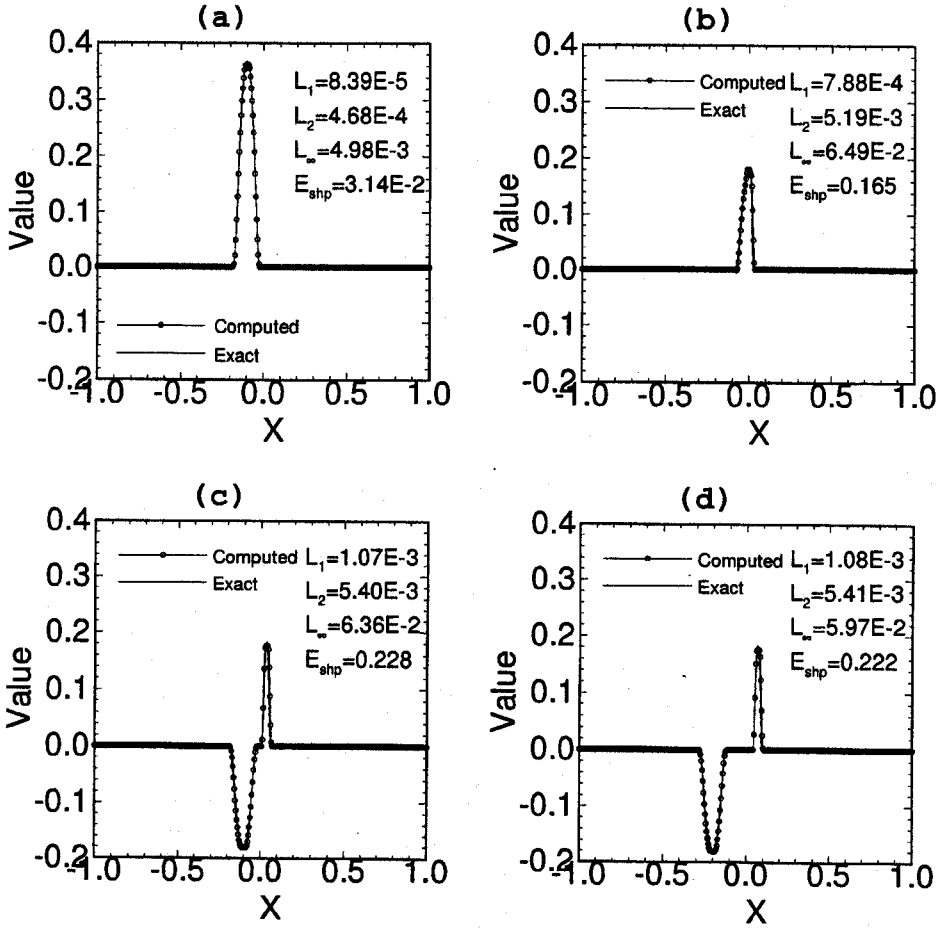

Fig. 10. The computed results for the case of $\rho_1 = \rho_2$ and $c_1 : c_2 = 1 : 1/3$. (a) $t = 0.1$; (b) $t = 0.2$; (c) $t = 0.3$; and (d) $t = 0.4$.

are also plotted in the same figure for the sake of comparison. An attribute of this figure is that the monotonically predicted solutions and the analytic data match well. This implies that, while the use of the FCT algorithm is regarded as a stabilizing ingredient, it results in only limited deterioration of accuracy.

We have also made an in-depth exploration of the influence of the fluid property on the quality of FCT solutions. To accomplish this task, we have considered different ratios of $c_2(x)/c_1(x)$, with fixed values of $\rho_2(x)/\rho_1(x) = 1:1$, namely 3, 1/2, 1/3. As indicated by Figs. 8–10, all of the solution profiles for p remain monotonic irrespective of the medium changes. It is clear that as the ratio of c_2/c_1 is smaller than 1, the solution profile is reflected out-of-phase from the interface.

7. Conclusions

A characteristic-based Taylor–Galerkin finite element model has been developed and applied to predict wave motion in layered fluids. Within this generalized framework, the free parameters α, β, γ and μ have been specifically chosen so that both leading dissipation and dispersion error terms are eliminated in the modified equation. The resulting high-order scheme, however, is subject to unstable oscillations and needs refinement. To circumvent this difficulty, we have incorporated the flux corrected transport technique of Boris and Book into the generalized Taylor–Galerkin finite element method. The key to the successful implementation of this filtering procedure lies in the accessibility of a low-order monotonic discretization scheme. To achieve this goal, we have proposed an explicit artificial viscosity model as a low-order solution by demanding that the resulting discrete system satisfies the TVD condition of Harten. We have tested three transport profiles propagating in a homogeneous linear hyperbolic system. Close agreement with analytic data has demonstrated the applicability of the high-order Taylor–Galerkin and low-order explicit artificial viscosity finite element methods to hyperbolic-type partial differential equations. The effectiveness of using the FCT technique to suppress local node-to-node oscillatory solutions has been demonstrated. The merits of the proposed finite element formulation have been appraised in this paper by using the second test problem. Numerical exercises have been made to show that this model is best suited to analyses involving discontinuous fluid properties. Both wave transmission and reflection can be well modeled.

Acknowledgments

The authors would like to thank the Computer Center of National Taiwan University and the National Center for High-performance Computing (NCHC) for the use of a CRAY J916 and an IBM RS/6000-590, respectively, which has made this study possible.

Appendix

In solving the governing Eq. (11), we can obtain its weak solution from the following

weighted residual statement:

$$\sum_{el=1}^{n_{el}} \int_{\Omega^{el}} \int_{t_n}^{t_{n+1}} \mathbf{W}(x) \left[\frac{\partial \phi}{\partial t} + \frac{\partial f}{\partial x} \right] dt d\Omega^{el} = 0 ,$$

where $\mathbf{W}(x)$ is the weighted function, Ω^{el} is the spatial domain of element el, and n_{el} is the total number of elements. t_n, t_{n+1} are the time steps at n and $n+1$, respectively. After performing the integration by parts, we have the following weak formulation:

$$\sum_{el=1}^{n_{el}} \int_{\Omega^{el}} \left[\mathbf{W}(x) \delta u^n - \frac{\partial \mathbf{W}(x)}{\partial x} \mathbf{I}(x) \right] d\Omega^{el} + [\mathbf{W}(x)\mathbf{I}(x)]|_\Gamma = 0 ,$$

where

$$\mathbf{I}(x) = \int_{t_n}^{t_{n+1}} f(x, t) dt .$$

By replacing the flux term $f(x, t)$ in the above equation with Taylor series expansion,[13] together with the use of the shape function defined in Eq. (14), we can get the matrix formulation described in Sec. 4. With the shape and weighted functions defined in Eq. (14), the values of element matrices can be calculated by applying the Gaussian quadrature integration technique. An element assemblage leads to the discretized equation for a node J, as shown in Eq. (15).

The procedure for deriving the modified equation is to apply Taylor series expansion. We expand the variables ϕ in Eq. (15) in a mesh which has been uniformly distributed, as follows:

$$\phi_{J+1}^n = \phi_J + \Delta x \phi_x|_J^n + \frac{1}{2}(\Delta x)^2 \phi_{xx}|_J^n + \frac{1}{6}(\Delta x)^3 \phi_{xxx}|_J^n + \frac{1}{24}(\Delta x)^4 \phi_{xxxx}|_J^n + \cdots$$

$$\phi_{J-1}^n = \phi_J - \Delta x \phi_x|_J^n + \frac{1}{2}(\Delta x)^2 \phi_{xx}|_J^n - \frac{1}{6}(\Delta x)^3 \phi_{xxx}|_J^n + \frac{1}{24}(\Delta x)^4 \phi_{xxxx}|_J^n - \cdots$$

$$\phi_J^{n+1} = \phi_J + \Delta t \phi_t|_J^n + \frac{1}{2}(\Delta t)^2 \phi_{tt}|_J^n + \frac{1}{6}(\Delta t)^3 \phi_{ttt}|_J^n + \frac{1}{24}(\Delta t)^4 \phi_{tttt}|_J^n + \cdots$$

$$\begin{aligned} \phi_{J+1}^{n+1} = {} & \phi_J + \Delta x \phi_x|_J^n + \Delta t \phi_t|_J^n + \frac{1}{2}(\Delta x)^2 \phi_{xx}|_J^n + \Delta x \Delta t \phi_{xt}|_J^n + \frac{1}{2}(\Delta t)^2 \phi_{tt}|_J^n \\ & + \frac{1}{6}(\Delta x)^3 \phi_{xxx}|_J^n + \frac{1}{2}(\Delta x)^2 \Delta t \phi_{xxt}|_J^n + \frac{1}{2}\Delta x (\Delta t)^2 \phi_{xtt}|_J^n + \frac{1}{6}(\Delta t)^3 \phi_{ttt}|_J^n \\ & + \frac{1}{24}(\Delta x)^4 \phi_{xxxx}|_J^n + \frac{1}{6}(\Delta x)^3 \Delta t \phi_{xxxt}|_J^n + \frac{1}{4}(\Delta x)^2 (\Delta t)^2 \phi_{xxtt}|_J^n \\ & + \frac{1}{6}\Delta x (\Delta t)^3 \phi_{xttt}|_J^n + \frac{1}{24}(\Delta t)^4 \phi_{tttt}|_J^n + \cdots \end{aligned}$$

$$\phi_{J-1}^{n+1} = \phi_J - \Delta x\phi_x|_J^n + \Delta t\phi_t|_J^n + \frac{1}{2}(\Delta x)^2\phi_{xx}|_J^n - \Delta x\Delta t\phi_{xt}|_J^n + \frac{1}{2}(\Delta t)^2\phi_{tt}|_J^n$$
$$- \frac{1}{6}(\Delta x)^3\phi_{xxx}|_J^n + \frac{1}{2}(\Delta x)^2\Delta t\phi_{xxt}|_J^n - \frac{1}{2}\Delta x(\Delta t)^2\phi_{xtt}|_J^n + \frac{1}{6}(\Delta t)^3\phi_{ttt}|_J^n$$
$$+ \frac{1}{24}(\Delta x)^4\phi_{xxxx}|_J^n - \frac{1}{6}(\Delta x)^3\Delta t\phi_{xxxt}|_J^n + \frac{1}{4}(\Delta x)^2(\Delta t)^2\phi_{xxtt}|_J^n$$
$$- \frac{1}{6}\Delta x(\Delta t)^3\phi_{xttt}|_J^n + \frac{1}{24}(\Delta t)^4\phi_{tttt}|_J^n + \cdots$$

Substitution of the above five relations into Eq. (15), together with the replacement of the temporal derivative terms with spatial derivative terms, enables us to derive the modified Eq. (16).

References

1. K. W. Morton, "Generalized Galerkin methods for hyperbolic problems," *Computer Methods in Applied Mechanics and Engineering* **52** (1985), 847–871.
2. P. Lesaint and P. A. Raviart, "On a finite element method for solving the neutron transport problem," in *Mathematical Aspects of Finite Elements in Partial Differential Equations*, ed. C. de Boor (Academic Press, 1974), pp. 89–123.
3. T. J. R. Hughes, M. Mallet and A. Mizukami, "A new finite element formulation for computational fluid dynamics: II. Beyond SUPG," *Computer Methods in Applied Mechanics and Engineering* **54** (1986), 341–355.
4. R. Löhner, K. Morgan and O. C. Zienkiewicz, "The solution of nonlinear systems of hyperbolic equations by the finite element method," *Int. J. Numer. Methods Fluids* **4** (1984), 1043–1063.
5. T. W. H. Sheu, C. C. Fang, S. H. Kuo and J. Y. Yang, "A high resolution capturing finite element method," *Proc. of 5th International Symposium on Computational Fluid Dynamics*, Tohoku University, Japan, ed. H. Daiguji **3** (1993), 103–108.
6. J. Donea, "A Taylor–Galerkin method for convective transport problems," *Int. J. for Numer. Meths. Engrg.* **20** (1984), 101–119.
7. A. Harten, "High resolution schemes for hyperbolic conservation laws," *J. Comp. Phys.* **49** (1983), 357–393.
8. A. Harten, "On a class of high resolution total-variation-stable finite difference schemes," *SIAM J. for Numerical Analysis* **21** (1983), 1–23.
9. J. P. Boris and D. L. Book, "Flux-corrected transport, I SHASTA, a fluid transport algorithm that works," *J. Comp. Phys.* **11** (1973), 38–69.
10. S. T. Zalesak, "Fully multidimensional flux-corrected transport algorithm for fluids," *J. Comp. Phys.* **31** (1979), 335–362.
11. G. Erlebacher, "Solution adaptive triangular meshes with application to the simulation of plasma equilibrium," Ph.D Thesis, Columbia University (1984).
12. A. K. Parrot and M. A. Christie, "Solution adaptive triangular meshes with application to the simulation of plasma equilibrium," in *Numerical Methods for Fluid Dynamics*, eds. K. W. Morton and M. J. Baines (Oxford University, 1986), pp. 609–620.
13. R. Löhner, K. Morgan, J. Peraire and M. Vahdati, "Finite element flux-corrected transport (FEM-FCT) for the Euler and Navier–Stokes equations," *Int. J. for Numer. Meths. in Fluids* **7** (1987), 1093–1109.